

Statistical Downscaling of Daily Temperatures and Precipitation Data from Coupled Model Inter-comparison Project 5 (CMIP5)-RCPs Experiment: In Weyib River Basin, Southeastern Ethiopia

Abdulkerim Bedewi Serur and Arup Kumar Sarma

Abstract Impact of climate change on the temperature and precipitation characteristics of Weyib River basin in Ethiopia has been investigated using CanESM2 model for the RCP2.6, RCP4.5, and RCP8.5 scenarios. The statistical downscaling model calibrated and validated using the observed daily data of 12 meteorological stations was used to generate the future scenario. The change in mean annual maximum temperature from the base period has indicated an increment of 0.16, 0.14, and 0.15 °C for RCP2.6, 0.12, 0.19, and 0.21 °C for RCP4.5, and 0.12, 0.22 and 0.32 °C for RCP8.5 for the 2020s, 2050s, and 2080s, respectively. Mean annual minimum temperature has shown an increment of 0.30, 0.43, and 0.39 °C for RCP2.6, 0.31, 0.48, and 0.57 °C for RCP4.5, and 0.34, 0.66 and 1.04 °C for RCP8.5 for the 2020s, 2050s and 2080s, respectively. For the percentage change in mean annual precipitation from the base period, the increment has been 8.68, 12.93, and 11.34% for RCP2.6, 9.54, 14.36, and 16.94% for RCP4.5, and 14.70, 19.14, and 28.69% for RCP8.5 for the 2020s, 2050s, and 2080s, respectively. There was a significantly (at 5% significant level) increasing trend of both temperatures and precipitation in all the three RCPs for future until the year 2100. The increment of rainfall in the study area was comparatively higher in the dry season 20.68% in the 2020s, 33.65% in 2050s, and 53.74% in 2080s for RCP8.5 which might have positive impact on pastoral region of the study area and it might affect the highland areas negatively since this season is expressly main crop harvesting period.

Keywords CMIP5-ESM-RCP experiment · SDSM · Climate change scenarios
Weyib river basin · Ethiopia

A.B. Serur (✉) · A.K. Sarma
Civil Engineering Department, Indian Institute of Technology Guwahati,
Guwahati 781039, Assam, India
e-mail: abdulkerimb1@gmail.com

A.K. Sarma
e-mail: aks@iitg.ernet.in

Introduction

It is observed that there is a substantial scale gap between what Global Circulation Models (GCMs) supply the predictors and what the hydrological models require climatic inputs to simulate hydrological processes. This scale discrepancy sources to a sizeable trouble for the valuation of climate change effect through hydrological models. Hence, significant awareness should be drawn to the development of downscaling methodologies so as to obtain local scale climate variables (mainly precipitation and temperatures) from coarse resolution ESMs. There are two prime methodologies accessible for the downscaling of large-scale resolution ESMs output to the finer (local) scale resolution (Wilby and Dawson 2007) namely dynamical (a higher resolution regional climate model is enforced to use ESMs output) and statistical (forms empirical relationships between large-scale atmospheric ESM variables, the predictors and local (finer or catchment) scale climate variables, the predictands) downscaling methodologies.

The projected mean annual temperature in Ethiopia are found to be in the ranges 0.9–1.1, 1.7–2.1, and 2.7–3.4 °C by 2030, 2050, and 2080 time slices, respectively (Ethiopian National Meteorological Agency 2007). The projected mean annual maximum and minimum temperature shows rising trend in southeastern part of Ethiopia (Shawul et al. 2016). The increment of large-scale mean surface temperature by the end of the twenty-first century are found to be in the ranges 2.6–4.8 °C (RCP8.5), 1.1–2.6 °C (RCP4.5), and 0.3–1.7 °C (RCP2.6) (IPCC 2013). In general, temperatures revealed an increasing trend (Kruger and Shongwe 2004; New et al. 2006; Unganai 1996) which tends to glacier to melt, sea level to rise, and alteration in circulation pattern which influence precipitation, water availability, and extremes of floods and droughts; just to name a few. There has been observed substantial variability in rainfall (rise about 20% and also declined by about 20%) in the globe (Bates et al. 2008). Larger spatial variation of precipitation (from a drop of about 25–50% to rise to 25–50%) has been reported in East Africa (Famarazi et al. 2013). Increase in rainfall has been observed (Shongwe et al. 2009) in the tropics. Rainfall variability is more in the African continent and resulted in variation in water availability. For instance, a decline in water availability (streamflow) (Beck and Bernauer 2011) by 2050s has been reported. Nevertheless, the rise of water availability (Graham et al. 2011) has also been stated. As we have seen in various literatures that there is an argument on the amount of decreasing or increasing of water availability on the globe.

The present unpredictable climate is a striking plenteous threat to Ethiopia by mainly disturbing water resources and agricultural sectors. Recent flooding incidences, as well as the widespread drought in Ethiopia, could remain placed as visible indications for these influences (Ethiopian National Meteorological Agency 2007). The Weyib River basin is used for several purposes (i.e., various water resources schemes involved to the flow of the river) but rises in temperature and change in rainfall magnitude and pattern affect the basin negatively. Therefore, in this study, statistical downscaling methodology using multiple linear regression

(MLR) based statistical downscaling model (SDSM) has been used to downscale daily temperatures (maximum and minimum) and precipitation data for 12 arbitrary meteorological stations found inside study area of Weyib River basin using CMIP5-CanESM2 for the RCP8.5, RCP4.5, and RCP2.6 scenarios. These future downscaled temperatures and precipitation data can be used as an input for hydrological models to simulate future, various surfaces, and subsurface hydrological processes. The analysis of future maximum and minimum temperature and precipitation was carried out on an annual, seasonal, and monthly basis for three (the 2020s; represents 2011–2040 time series data, 2050s; represents 2041–2070 time series data and 2080s; represents 2071–2100 time series data) time slices in future periods.

Materials and Methods

Study Area (Weyib River Basin)

The Weyib River basin (Fig. 1) has an area of 4215.93 km² and is situated between 6.50 and 7.50°N latitude and 39.50–41.00°E longitude. The altitude variation ranges around 4389 m (a.m.s.l.) at the highest point to 898 m at the confluence point. Mean annual maximum and minimum temperature of the study area are 22.30 and 7.60 °C, respectively. The average rainfall in the study area ranges 749.34–1368.90 mm (mean of 1037.40 mm) per annum. The Eutric Vertisol and Dystric Cambisol are the two main soil types, and agriculture is a leading land use type. Roughly, 70.54% of the basin area covered with 0–15% land slope. Mean annual total water availability (in the simulation period 1984–2004) has to be 553.46 mm.

Earth System Model (ESM) and RCP Scenarios

In this study, a bias-corrected CMIP5-ESMs climate model for the RCP8.5 (very high emission scenario), RCP4.5 (an intermediate emission scenario), and RCP2.6 (very low emission scenario) scenarios has been used. The historical and future predictor variables have been downloaded through official website (<http://ccds-dscc.ec.gc.ca/?page=pred-canesm2>) of Canadian Centre for Climate Modelling and Analysis (<http://ccds-dscc.ec.gc.ca/?page=pred-canesm2CCCMA>). These predictors are assigned in zip file format and have five files inside (CanESM2_historical_1961-2005, CanESM2_rcp26_2006-2100, CanESM2_rcp45_2006-2100, CanESM2_rcp85_2006-2100 and NCEP-NCAR_1961-2005) the predictors prepared, this technique was used as an input in SDSM.

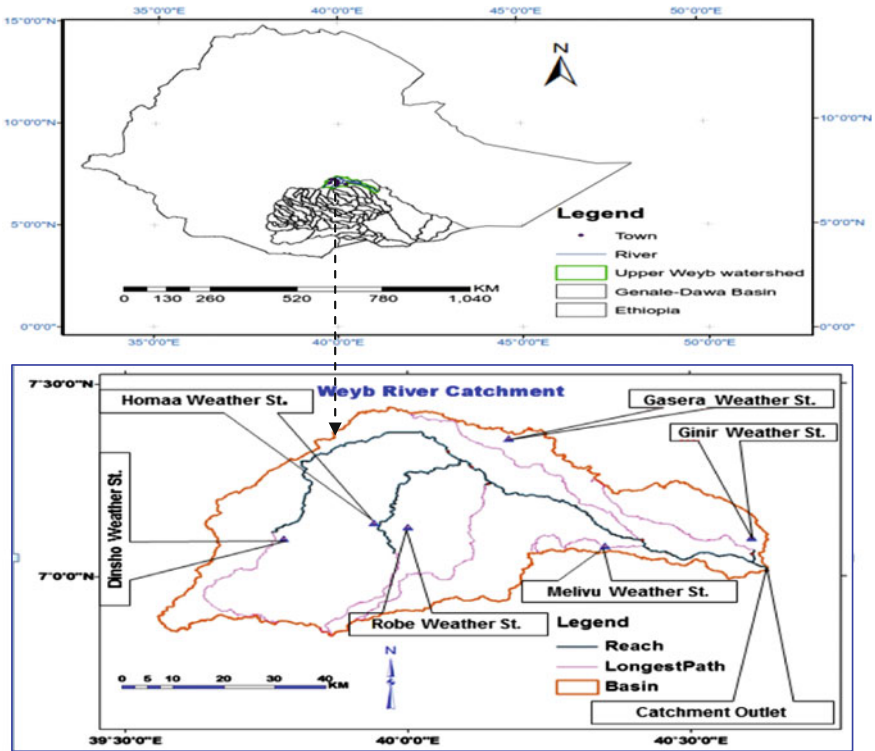


Fig. 1 Study area: location map, reach, basin, and selected weather stations of the Weyib River basin

Types of Data Used

Daily weather data and ESM data were utilized for this study. The daily weather data (daily precipitation, Tmax, Tmin, mean wind speed, relative humidity and sunshine hours) for 12 weather stations (detailed in Table 1) were collected from National Meteorological Service Agency of Ethiopia (NMSA). The source of ESM data is the official website of Canadian Centre for Climate Modelling and Analysis mentioned above in ‘earth system model (ESM) and RCP Scenarios’ section. The mean monthly rainfall (mm) and temperature (°C) characteristics of Weyib River basin are depicted in Fig. 2.

Table 1 Details of the 12 meteorological stations and their data records

S. No.	Station name	Data recording periods	Latitude (°N)	Longitude (°E)	Altitude (m)	Total annual mean precipitation (mm)	Mean annual max. temp (°C)	Mean annual min. temp (°C)
1	Robe	1984–2011	7.133	40.000	2464	804.14	21.79	8.00
2	Goba	1998–2007	7.017	40.000	2613	980.03	20.13	6.52
3	Dinsho	1981–2007	7.100	39.783	3072	1368.90	17.43	3.43
4	Agarfa	1988–1997	7.267	39.817	2465	762.36	22.38	8.13
5	Sinnana	1982–2008	7.067	40.217	2364	894.35	21.39	8.02
6	Adaba	1980–2010	7.000	39.383	2415	823.65	23.87	5.10
7	Homa	1988–2010	7.133	39.933	2505	846.58	21.75	7.33
8	Ali	1988–2005	7.017	40.350	2460	1264.17	20.47	6.68
9	Gassera	1980–2010	7.367	40.183	2337	1181.12	20.67	6.95
10	Goro	1981–2005	7.000	40.467	1806	887.14	26.77	7.89
11	Ginnir	1980–2012	7.133	40.700	1929	1030.04	23.82	13.20
12	Hunte	1980–2011	7.100	39.417	2413	749.34	23.71	6.73

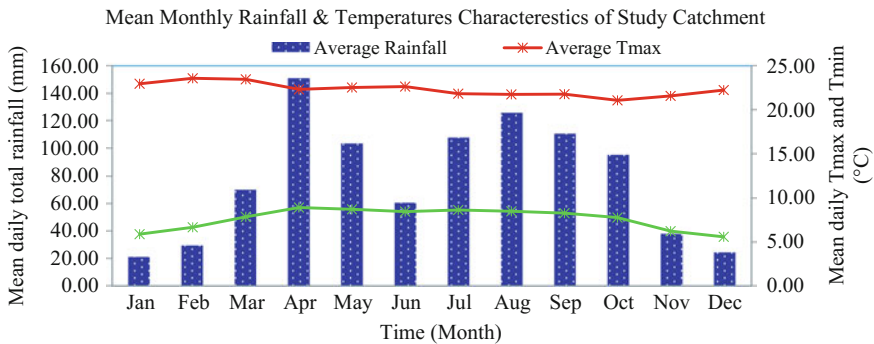


Fig. 2 Mean (12 stations) monthly rainfall and temperature characteristics of Weyib River basin

Downscaling Methods

There are two prime methodologies accessible for the downscaling of large-scale spatial ESMs output to the local scale spatial resolution (Wilby and Dawson 2007) namely dynamical (a higher resolution regional climate model is enforced to use ESMs output) and statistical downscaling methodologies. The statistical downscaling method establishes empirical relationships between large-scale ESM outputs, the predictors, and local scale climatic variables (for instance, Tmax, Tmin, and precipitation), the predictands with the help of some transfer function as shown in the following relation.

$$Y = f(X), \quad (1)$$

where Y is local Tmax, Tmin, and precipitation that were being downscaled, X stands for a set of large-scale potential predictor variables (for instance, mean sea level pressure, geopotential heights and specific humidity at the surface and 850 hpa), and f represents a stochastic function that relates the predictands and predictors.

The “ f ” function is determined empirically from historical observations by training and validating the model. Thus, the achievement of the statistical downscaling method was based on the relationship used and choice of potential predictor variables, whose performance can be verified through estimation of various statistical indices (for instance, R^2 , RMSE, and NSE). It is roughly divided into three classes (weather typing, weather generators, and regression-based downscaling). Regression analysis is very powerful for forecasting (Ghosh and Mujumdar 2008); it is divided into two categories namely simple regression and multiple regressions. The statistical downscaling method has its own merits and demerits. Key demerits of statistical downscaling contain the assumption that observed relations between large-scale predictors and local predictands will continue in a changing climate. Similarly, some merits of statistical downscaling contain: it is easy to apply, has the possibility to downscale from many ESMs and different emission scenarios, and downscales comparatively fast and inexpensive. Therefore, in this study, the independent variables are more than one, so MLR using SDSM has been used to downscale daily temperatures and precipitation data from Ensembles of ESM for the future RCP scenarios.

Statistical Downscaling Model (SDSM)

The SDSM can perform a combination of the stochastic weather generator and regression-based on the family of the transfer function (Liu et al. 2011). It performs the spatial downscaling through daily predictor–predictand relationships using MLR and creates predictands that represent the local weather condition. Regression-based in the family of transfer function method is the well-known technique of downscaling (Ghosh and Mujumdar 2008) that depends on the direct, measurable link between predictand and predictors through some form of regression. SDSM version 4.2.9 a decision support tool (Wilby and Dawson 2007) has been used for this study to downscale daily future Tmax, Tmin, and precipitation. This model was downloaded from the website <http://co-public.lboro.ac.uk/cocwd/SDSM/>. There are seven major steps to be followed in developing the best performing MLR equation for the downscaling processes in this version of SDSM. Detailed discussions of the steps are given in (Wilby et al. 2002; Wilby and Dawson 2007).

The choice of appropriate downscaling potential predictor variables has been done with the help of the screen variables option of the SDSM using correlation analysis, partial correlation analysis, and scatter plot. Screening the potential predictors has been done through choosing seven or eight predictors at a time and their explained variance has been analyzed, thereby choosing those predictors which have greater explained variance and drop the rest. Then partial correlation analysis has been done for nominated predictors to see the level of association with each other; these statistics identify the extent of the descriptive power of the predictor to describe the predictand. Therefore, the predictors used for downscaling should be reliably generated by ESMs, freely accessible from ESM outputs archive and strongly linked with the local climate variables of concern (Tmax, Tmin, and precipitation in this case).

The calibration process in SDSM constructs downscaling model based on MLR equations, with given daily station wise weather data (predictand) and potential predictors. The model calibration operation has been run for station wise precipitation, Tmax and Tmin along with a set of possible predictor variables, and computes the parameters of MLR equations through an optimization algorithm (Dual simplex has used in this case). SDSM's weather generator enables to produce ensembles of synthetic current daily weather data based on inputs of the measured time series data and the MLR parameters generated during the calibration step. Finally, station wise Tmax, Tmin, and precipitation scenario have been generated until the year 2100 using CMIP5-CanESM2 model outputs (potential predictor variables for the future period) for the RCP8.5, RCP4.5, and RCP2.6 emission scenarios. Twenty ensembles of synthetic daily Tmax, Tmin and precipitation time series data were generated for the period from 2006 to 2100 for all stations and the mean of these 20 ensembles was used as final daily Tmax, Tmin, and precipitation data for the stated period. Moreover, then the future Tmax, Tmin, and precipitation scenarios have been established by dividing the later date series into three (the 2020s, 2050s, and 2080s) time slices for the 12 averaged arbitrary spatial weather stations.

Precipitation and Temperatures Scenario Statistics

Percentage and absolute change have been used to calculate three-time slices of 30 years precipitation and temperatures, respectively.

A percentage change has been used for precipitation;

$$\Delta_{2020s} = \frac{(V_{2020s} - V_{base}) \times 100}{V_{base}} \quad (2)$$

$$\Delta_{2050s} = \frac{(V_{2050s} - V_{base}) \times 100}{V_{base}} \quad (3)$$

$$\Delta 2080s = \frac{(V2080s - Vbase) \times 100}{Vbase}. \quad (4)$$

Absolute difference has been used for temperatures,

$$\Delta 2020s = V2020s - Vbase \quad (5)$$

$$\Delta 2050s = V2050s - Vbase \quad (6)$$

$$\Delta 2080s = V2080s - Vbase, \quad (7)$$

where, Vbase is the mean of 20 ensembles of Tmax, Tmin and precipitation for the base period for each ESM-RCP and each station. V2020s, V2050s, and V2080s are the average of 20 ensembles of Tmax, Tmin, and precipitation for the period of 2011–2040, 2041–2070, and 2071–2100, respectively, for each ESM-RCP experiment and each station.

Mann–Kendall Trend Test

A nonparametric rank-based procedure has frequently been used to evaluate if there is a rise or decline trend in the time series of meteorological and hydrological data (Hamed 2008; Karpouzou et al. 2010). The Mann–Kendall test was applied in this study to see the existing trends (rise or decline) of Tmax, Tmin, and precipitation for the RCP8.5, RCP4.5, and RCP2.6 scenarios in future periods.

SDSM Performance Evaluation

In order to evaluate the SDSM performance relative to the observed Tmax, Tmin, and precipitation data, the following three statistical model performance evaluation measures, in addition to graphical technique, were used during the calibration and validation periods.

Coefficient of Determination (R^2)

It was given by (Krause and Boyle 2005) as shown in Eq. 8

$$R^2 = \frac{(\sum[Xi - Xav][Yi - Yav])^2}{\sum(Xi - Xav)^2 \sum(Yi - Yav)^2}, \quad (8)$$

where, X_i is measured value, X_{av} is average measured value, Y_i is simulated value, and Y_{av} is average simulated value.

Nash–Sutcliffe Coefficient (E)

It was given by (Nash and Sutcliffe 1970) as shown in Eq. 9

$$E = 1 - \frac{\sum_{i=1}^n (X_{obs,i} - X_{model})^2}{\sum_{i=1}^n (X_{obs,i} - \bar{X}_{obs})^2}, \quad (9)$$

where X_{obs} is observed values and X_{model} is modeled values at time/place i .

Root Mean Square Error (RMSE)

It was given by (Singh et al. 2004) as shown in Eq. 10

$$RMSE = \sqrt{\frac{\sum_{i=1}^n (X_{obs,i} - X_{model,i})^2}{n}}, \quad (10)$$

where X_{obs} is observed values, X_{model} is modeled values at time/place i , and n is number of observation.

Results and Discussion

Selected Potential Predictor Variables

The lists of selected common potential predictor variables in the entire basin that gave better correlation results at $p < 0.05$ for CanESM2 are listed in Table 2.

Results revealed that different atmospheric variables affect different local variables. For instance, precipitation is more sensitive to mean sea level pressure, specific humidity (at surface and 850 hPa), zonal velocity (at 500 and 850 hPa), and geopotential heights (at 500 hPa). Mean sea level pressure, geopotential heights (at 500 and 850 hPa), average temperature (at 2 m height), specific humidity (at near surface and 850 hPa), and wind direction (at 850 hPa) affect both the maximum and minimum temperature under the CanESM2-historical model.

Table 2 List of selected potential predictor variables that provided better correlation results at $p < 0.05$ from CanESM2-historical model for study area of Weyib River basin

Predictand	Predictor full name	Notations	Parti.cor. (<i>r</i> -value)	<i>p</i> -value
Precipitation	Mean sea level pressure	ceshmslpgl.dat	0.050	0.020
	Specific humidity at 850 hPa	ceshs850gl.dat	0.090	0.000
	Surface specific humidity	ceshshumgl.dat	0.077	0.002
	500 hPa zonal velocity	ceshp5_ugl.dat	-0.094	0.000
	850 hPa zonal velocity	ceshp8_ugl.dat	-0.119	0.000
	500 hPa geopotential height	ceshp500gl.dat	0.056	0.016
Maximum temperature	Mean sea level pressure	ceshmslpgl.dat	0.148	0.000
	500 hPa geopotential height	ceshp500gl.dat	0.134	0.000
	Specific humidity at 850 hPa	ceshs850gl.dat	-0.268	0.000
	Mean temperature at 2 m	ceshtempgl.dat	-0.235	0.000
	850 hPa wind direction	ceshp8thgl.dat	0.110	0.000
	850 hPa geopotential height	ceshp850gl.dat	-0.200	0.000
	Surface specific humidity	ceshshumgl.dat	-0.274	0.000
Minimum temperature	Mean sea level pressure	ceshmslpgl.dat	-0.308	0.000
	500 hPa geopotential height	ceshp500gl.dat	0.222	0.000
	Surface specific humidity	ceshshumgl.dat	0.146	0.000
	Mean temperature at 2 m	ceshtempgl.dat	0.323	0.000
	Specific humidity at 850 hPa	ceshs850gl.dat	-0.116	0.000
	850 hPa geopotential height	ceshp850gl.dat	-0.103	0.000
	850 hPa wind direction	ceshp8thgl.dat	0.078	0.000
	850 hPa zonal velocity	ceshp8_ugl.dat	-0.116	0.000

Note The partial correlation coefficient (*r*) shows the explanatory power that is specific to each predictor. All are significant at $p \leq 0.05$. *hpa* is a unit of pressure, 1 hPa = 1 mbar = 100 Pa = 0.1 kPa

Calibration and Validation of SDSM for Both Temperatures and Precipitation

For downscaling of maximum temperature and minimum temperature, and precipitation MLR, using SDSM, was used to calibrate and validate the model. The entire length of the observed data was available from 1981 to 2005. This data was divided into two parts for calibration and validation. Data from 1981 to 1993 was used for the calibration whereas data from 1994 to 2005 was used for the validation of the model.

Calibration and validation results for 12 averaged spatial stations maximum temperature downscaling model are shown in (Fig. 3a, b). The coefficients of determination (R^2), RMSE and NSE values were 0.95, 0.44, and 0.79, respectively, for calibration period whereas R^2 , RMSE and NSE values of 0.94, 0.46, and 0.82, respectively, for validation period. For minimum temperature (Fig. 3c, d), the R^2 , RMSE, and NSE values were 0.92, 0.58, and 0.86, respectively, for calibration period whereas R^2 , RMSE, and NSE values were 0.93, 0.58, and 0.88 for validation period. Calibration and validation results for 12 averaged spatial stations precipitation downscaling model are shown in (Fig. 3e, f). The R^2 , RMSE, and NSE values were 0.83, 0.98, and 0.78, respectively, for calibration period whereas R^2 , RMSE, and NSE values of 0.86, 0.79, and 0.84, respectively for validation period.

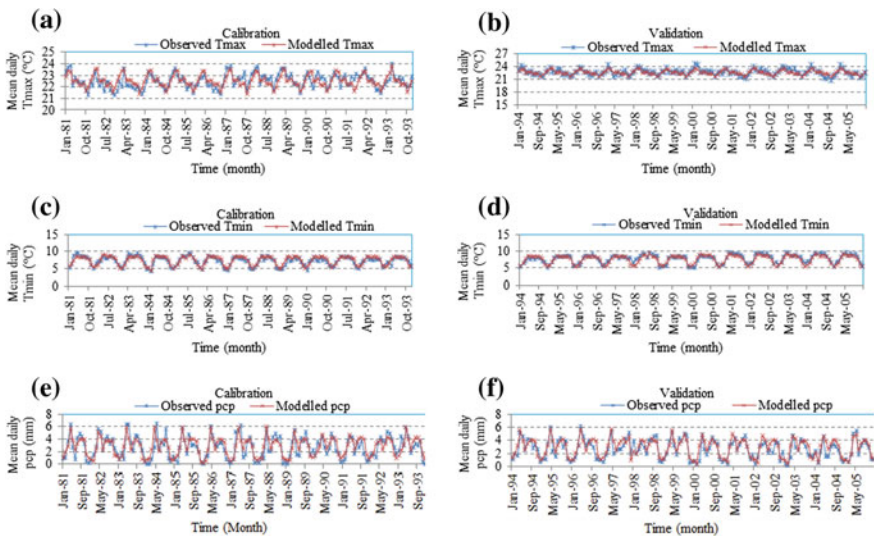


Fig. 3 a Calibration result of SDSM for maximum temperature from average of 3 ESMs (1981–1993) (upper left), b same as (a) but for validation period (1994–2005) (upper right), c calibration result of SDSM for minimum temperature (middle left), d same as (c) but for validation period (middle right), e calibration result of SDSM for precipitation (bottom left), f same as (e) but for validation period (bottom right)

From these results, we can argue that the model is well performed for the maximum and minimum temperature, and precipitation downscaling for both calibration and validation period.

Scenarios Developed for Future Temperatures and Precipitation

Maximum Temperature Scenarios

The projected mean seasonal maximum temperature shows a decreasing trend in the dry season in all the three future time slices for RCP2.6, RCP4.5, and RCP8.5 scenarios except for RCP2.6 scenario which is an increasing trend in the dry season of the 2020s. However, it has shown an increasing trend for both an intermediate and wet seasons in all the three future time slices for RCP2.6, RCP4.5, and RCP8.5 scenarios except for RCP2.6 scenario which is a decreasing trend in a wet season of the 2020s. The absolute changes of maximum temperature from the base period for three scenarios in future time slice for each season are presented in Table 3.

The projected mean monthly maximum temperature has a larger magnitude of increment on the month of June 2080s which was 0.58, 0.80, and 1.37 °C for RCP2.6, RCP4.5, and RCP8.5 scenarios, respectively. On the other hand, the larger decrement on December 2080s 0.75, 0.38 °C, and on December 2050s 0.32 °C occurred for RCP8.5, RCP4.5, and RCP2.6 scenarios, respectively (Figs. 4, 5 and 6). The absolute change in mean maximum temperature was observed to be sizable due to a substantial increase and decrease of maximum temperature on different months. For instance, in the months of January, February, November, and December, the decrement of the maximum temperature was observed and an increment on the rest of the months was observed.

Generally, the change in average monthly maximum temperature might range between -0.25 °C on December and $+0.48$ °C on June for the coming 2020s (2011–2040); -0.50 °C on December and $+0.91$ °C on June for 2050s (2041–2070) and -0.75 °C on December and $+1.37$ °C on June for 2080s (2071–2100) for the RCP8.5 scenario. The change in average monthly maximum temperature for RCP4.5 scenario varies between -0.25 °C on December and $+0.47$ °C June for the coming 2020s; -0.33 °C on December and $+0.70$ °C on June for 2050s and -0.38 °C on December and $+1.37$ °C on June for 2080s. For RCP2.6, ranges -0.12 °C on August and $+0.42$ °C on December for 2020s; -0.32 °C on December and $+0.58$ °C on June for 2050s and -0.28 on December and $+0.55$ °C on June for 2080s.

For each time slice, the change in mean annual maximum temperature has indicated a slight increment from the base period, 0.16, 0.14, and 0.15 °C for 2020s, 2050s, and 2080s, respectively, for RCP2.6 scenario, 0.12, 0.19, and 0.21 °C for 2020s, 2050s, and 2080s, respectively, for RCP4.5 scenario, and 0.12, 0.22, and 0.33 °C for 2020s, 2050s, and 2080s, respectively, for RCP8.5 scenario.

Table 3 Absolute change in mean seasonal maximum temperature (°C) at different time horizons from the base period

Scenario	Seasons in the 2020s			Seasons in the 2050s			Seasons in the 2050s		
	Dry	Intermediate	Wet	Dry	Intermediate	Wet	Dry	Intermediate	Wet
CanESM2-RCP2.6	+0.275	+0.194	-0.002	-0.017	+0.228	+0.215	-0.002	+0.224	+0.208
CanESM2-RCP4.5	-0.012	+0.192	+0.167	-0.001	+0.301	+0.257	-0.001	+0.338	+0.283
CanESM2-RCP8.5	-0.007	+0.202	+0.168	-0.036	+0.370	+0.326	-0.051	+0.529	+0.495

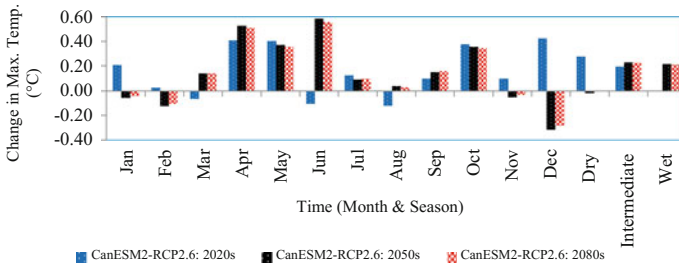


Fig. 4 Change in average monthly and seasonal maximum temperature in the future from the base period for CanESM2-RCP2.6 scenario

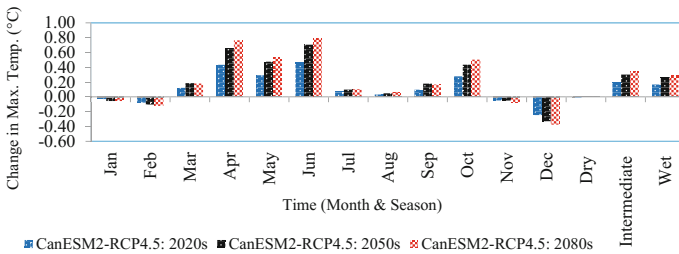


Fig. 5 Change in average monthly and seasonal maximum temperature in the future from the base period for CanESM2-RCP4.5 scenario

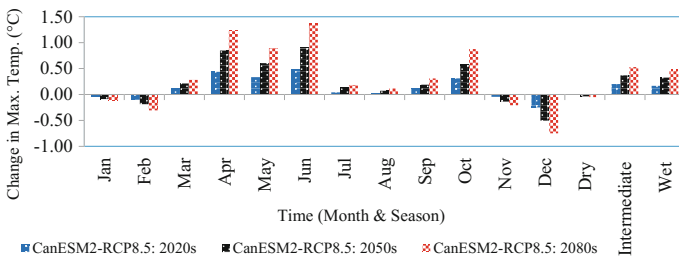


Fig. 6 Change in average monthly and seasonal maximum temperature in the future from the base period for CanESM2-RCP8.5 scenario

The variability of maximum temperature is higher for RCP8.5 than RCP4.5 and RCP2.6, and the linear trend line for three scenarios has indicated a significantly (at 5% significant level) increasing trend of average annual maximum temperature until the end of the century (Table 6 and Fig. 7). Comparatively, RCP8.5 (very high emission scenario) prevails higher change in maximum temperature trend at the end of the century than the RCP4.5 (an intermediate emission scenario) and RCP2.6 (very low emission scenario).

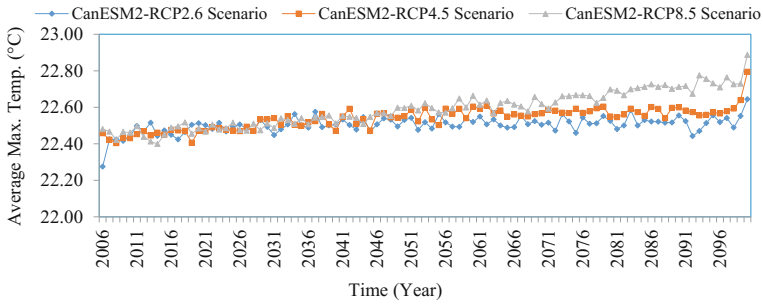


Fig. 7 Future pattern of average annual maximum temperature

Minimum Temperature Scenarios

The projected mean seasonal minimum temperature shows an increasing trend in all the seasons (Dry, intermediate, and wet) in all the three future time horizons for all the RCP (RCP2.6, RCP4.5, and RCP8.5) scenarios. The changes of minimum temperature from the base period for the three scenarios in future time slice for each season are presented in Table 4. The projected mean monthly minimum temperature has a larger magnitude of increment on the month of October 2080s which was 2.13, 1.24, and 0.95 °C for RCP8.5, RCP4.5, and RCP2.6 scenarios, respectively, at the end of the century. On the other hand, the larger decrement on February 2080s 0.51, 0.48, and 0.36 °C occurred for RCP8.5, RCP4.5, and RCP2.6 scenarios, respectively, at the end of the century (Figs. 8, 9 and 10). The absolute change from the base period in mean minimum temperature was observed to be significant due to a substantial increase and decrease of minimum temperature on different months. For instance, in the months of February, September, and December, the decrement of the minimum temperature was observed and an increment on the rest of the months was observed. In both extreme conditions (rise or decline), the change in minimum temperature was higher in the 2080s.

Commonly, the change in average monthly minimum temperature might range between -0.30 °C on February and +0.87 °C on October for the coming 2020s; -0.41 °C on February and +1.38 °C on October for 2050s and -0.51 °C on February and +2.13 °C on October for 2080s for the RCP8.5 scenario. For RCP4.5 scenario, it varies between -0.32 °C on February and +0.69 °C on October for the coming 2020s; -0.42 °C on February and +1.12 °C on October for 2050s and -0.48 °C on February and +1.24 °C on October for 2080s. For RCP2.6 scenario, ranges become -0.30 °C on February and +0.74 °C on October for the 2020s; -0.31 °C on February and +0.94 °C on October for 2050s and -0.36 °C on February and +0.95 °C on October for 2080s.

For each time slice, the change in mean annual minimum temperature has indicated a slight increment from the base period, 0.30, 0.43, and 0.39 °C for 2020s, 2050s, and 2080s, respectively, for RCP2.6 scenario, 0.31, 0.48, and 0.57 °C for 2020s, 2050s, and 2080s, respectively, for RCP4.5 scenario and 0.34,

Table 4 Absolute change in mean seasonal minimum temperature ($^{\circ}\text{C}$) at different time horizons from the base period

Scenario	Seasons in the 2020s			Seasons in the 2050s			Seasons in the 2050s		
	Dry	Intermediate	Wet	Dry	Intermediate	Wet	Dry	Intermediate	Wet
CanESM2-RCP2.6	+0.307	+0.371	+0.213	+0.431	+0.544	+0.303	+0.418	+0.467	+0.283
CanESM2-RCP4.5	+0.299	+0.390	+0.240	+0.488	+0.598	0.354	+0.567	+0.702	+0.431
CanESM2-RCP8.5	+0.366	+0.425	+0.238	+0.682	+0.809	+0.473	+1.090	+1.332	+0.702

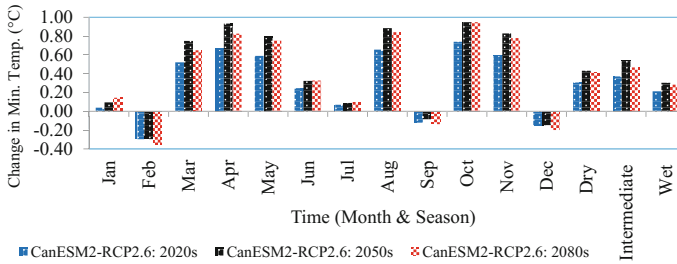


Fig. 8 Change in average monthly and seasonal minimum temperature in the future from the base period for CanESM2-RCP2.6 scenario

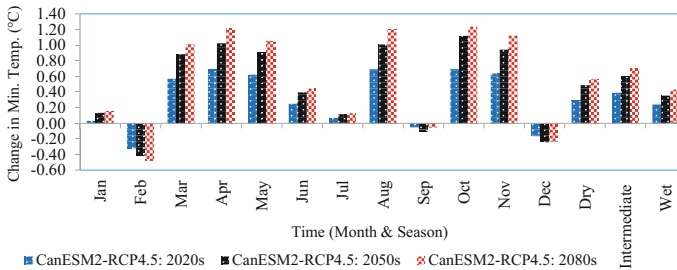


Fig. 9 Change in average monthly and seasonal minimum temperature in the future from the base period for CanESM2-RCP4.5 scenario

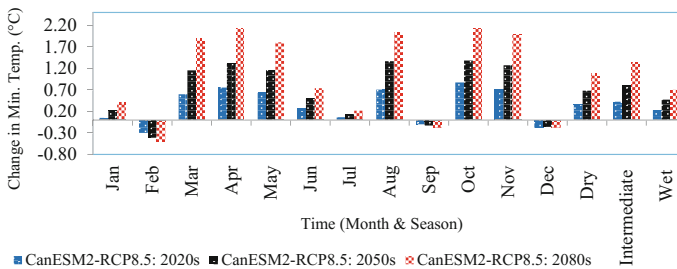


Fig. 10 Change in average monthly and seasonal minimum temperature in the future from the base period for CanESM2-RCP8.5 scenario

0.66, and 1.04 °C for 2020s, 2050s, and 2080s, respectively, for RCP8.5 scenario. The variability of minimum temperature is higher for RCP8.5 than RCP4.5 and RCP2.6, and the linear trend line for three scenarios has indicated a significantly (at 5% significant level) increasing trend of average annual minimum temperature until the end of the century (Table 6 and Fig. 11). Comparatively, RCP8.5 prevails higher change in minimum temperature trend at the end of the century than the

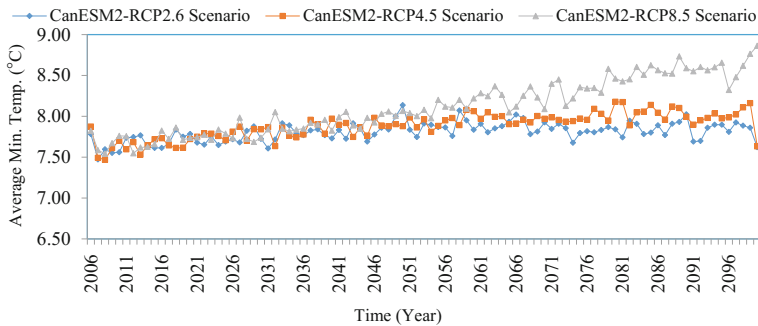


Fig. 11 Future pattern of average annual minimum temperature

RCP4.5 and RCP2.6 scenarios. The future scenarios have shown slightly increasing trend on both maximum and minimum temperature.

The results of average temperature for this study come to an agreement, with the slight variation of RCP8.5 scenario, with the study reported (IPCC 2013) and the results revealed the rise in global average surface temperature by the end of the twenty-first century to be in the ranges 2.6–4.7, 1–2.5, and 0.3–1.6 °C for the RCP8.5, RCP4.5, and RCP2.6 scenarios, respectively. The projected mean annual temperature in Ethiopia was found to be in the ranges 0.9–1.1, 1.7–2.1, and 2.7–3.4 °C by 2030, 2050, and 2080 time slices, respectively (Ethiopian National Meteorological Agency 2007). The projected mean annual maximum and minimum temperature show rising trend in southeastern part of Ethiopia (Shawul et al. 2016). The mean annual temperature of this study comes to an agreement with all the literature given above regarding direction (pattern), but with slight variation regarding magnitude (amount). This slight variation of mean annual temperature increment might arise due to the types of GCM/ESM and emission scenario used, a method of downscaling, and spatial variation of temperature.

Precipitation Scenarios

The projected mean seasonal precipitation scenarios have indicated an increase of precipitation in all the seasons (Dry, intermediate, and wet) in all the three future time slices for RCP2.6, RCP4.5, and RCP8.5 scenarios except for an intermediate period of the 2020s (a decreasing trend) for RCP2.6 and RCP4.5 scenarios. The percentage changes of precipitation from the base period for the three scenarios in future time horizon for each season are presented in Table 5.

The projected mean monthly precipitation has a larger magnitude of increment on the month of October 2080s 81.02, 54.66, and 42.77% for RCP8.5, RCP4.5, and RCP2.6 scenarios, respectively, at the end of the century. Conversely, the larger decrement on February 2020s 8.20 (‘RCP8.5’), 10.25% (‘RCP4.5’), and 10.90% (‘RCP2.6’) was observed (Figs. 12, 13 and 14). The percentage change from the

Table 5 Percentage difference in mean seasonal precipitation at different time horizons from the base period

Scenario	Seasons in the 2020s			Seasons in the 2050s			Seasons in the 2050s		
	Dry	Intermediate	Wet	Dry	Intermediate	Wet	Dry	Intermediate	Wet
CanESM2-RCP2.6	+15.19	-1.35	+8.83	+24.11	+2.57	+11.44	+21.14	+1.02	+9.81
CanESM2-RCP4.5	+18.20	-0.32	+9.16	+26.63	+1.96	+13.50	+30.71	+4.55	+15.65
CanESM2-RCP8.5	+20.68	+1.37	+9.10	+33.65	+6.23	+18.85	+53.74	+18.90	+27.06

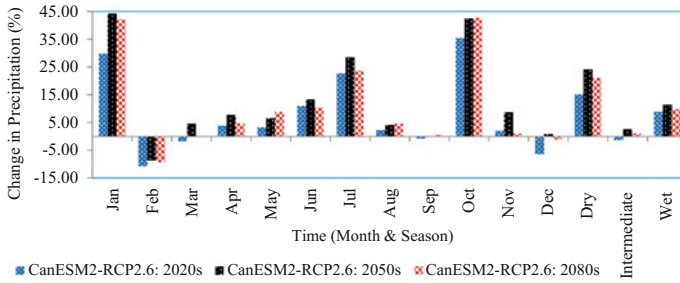


Fig. 12 Percentage change in average monthly and seasonal precipitation in the future from the base period for CanESM2-RCP2.6 scenario

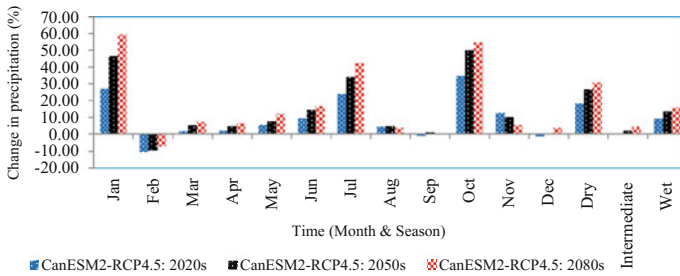


Fig. 13 Percentage change in average monthly and seasonal precipitation in the future from the base period for CanESM2-RCP4.5 scenario

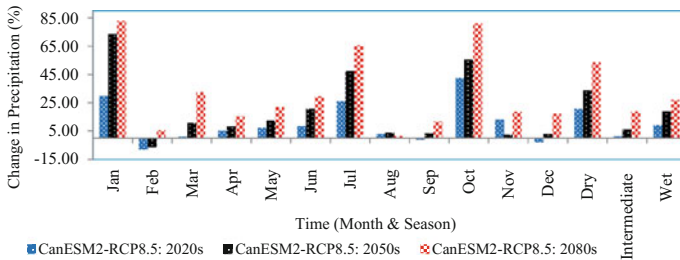


Fig. 14 Percentage change in average monthly and seasonal precipitation in the future from the base period for CanESM2-RCP8.5 scenario

base period in mean monthly precipitation was observed to be significant due to a substantial rise and decline of precipitation on different months. For instance, in the months of February, September, and December, the decrement of precipitation was observed and an increment in the rest of the months was shown.

Characteristically, the percentage change in average monthly precipitation might range between -8.20% on February and $+42.59\%$ on October for the coming

2020s; -6.50% on February and +55.61% on October for 2050s and +1.58% on August and +81.02% on October for 2080s for the RCP8.5 scenario. For RCP4.5 scenario, the range tends to be between -10.35% on February and +34.53% on October for the coming 2020s; -9.36% on February and +49.90 on October for 2050s and -7.42% on February and +54.66% on October for 2080s. For RCP2.6 scenario, percentage change in average monthly precipitation ranges between -10.80% on February and +35.41% on October for 2020s; -8.59% on February and +42.55% on October for 2050s and -9.37% on February and +42.77% on October for 2080s.

For each time slice, the percentage change in mean annual precipitation has indicated a considerable increment from the base period, 8.68, 12.93, and 11.34% for 2020s, 2050s, and 2080s, respectively, for RCP2.6 scenario, 9.54, 14.36, and 16.94% for 2020s, 2050s, and 2080s, respectively for RCP4.5 scenario and 14.70, 19.14, and 28.69% for 2020s, 2050s, and 2080s, respectively, for RCP8.5 scenario. The variability of precipitation is higher for RCP8.5 than RCP4.5 and RCP2.6, and the linear trend line for three scenarios has indicated a significantly (at 5% significant level) increasing trend of average annual total precipitation until the end of the century (Table 6 and Fig. 15). Comparatively, RCP8.5 prevails higher change in precipitation trend at the end of the century than the RCP4.5 and RCP2.6 scenarios.

Figure 15 indicated the pattern of future total mean annual precipitation with a range of 1124.00–1540.16 mm in the year 2028 and 2099, respectively, for RCP8.5 scenario, 1065.43–1359.59 mm in the year 2018 and 2064, respectively, for RCP4.5 scenario and 1100.74–1300.24 mm in the year 2096 and 2050, respectively, for RCP2.6 scenario. It has shown the substantial variability of total mean annual precipitation from year to year throughout simulation period. There has been observed substantial variability in rainfall (rises about 20% and also declined by about 20%) in the globe (Bates et al. 2008). Larger spatial variation of precipitation (from a reduction of 25–50% to an increase of 25–50%) has been reported in East Africa (Faramarzi et al. 2013). Increase in rainfall has been observed

Table 6 Mann–Kendall trend test for future average annual both temperatures and precipitation under three RCP scenarios

scenarios	Kendall’s tau	p-value	Alpha	Sen’s slope	Trend
Tmax for rcp2.6	0.492	<0.0001	0.05	0.117	Significantly increasing
Tmax for rcp4.5	0.521	<0.0001	0.05	0.117	Significantly increasing
Tmax for rcp8.5	0.634	<0.0001	0.05	0.211	Significantly increasing
Tmin for rcp2.6	0.196	<0.0001	0.05	0.106	Significantly increasing
Tmin for rcp4.5	0.256	<0.0001	0.05	0.109	Significantly increasing
Tmin for rcp8.5	0.435	<0.0001	0.05	0.118	Significantly increasing
pcp for rcp2.6	0.186	0.0003	0.05	0.378	Significantly increasing
pcp for rcp4.5	0.193	0.0005	0.05	0.546	Significantly increasing
pcp for rcp8.5	0.201	0.0009	0.05	0.607	Significantly increasing

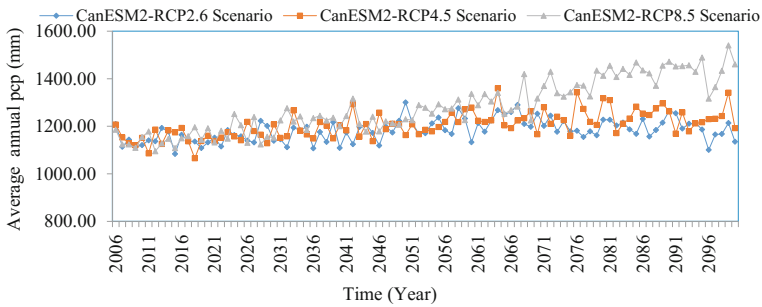


Fig. 15 Future pattern of average annual total precipitation

(Shongwe et al. 2009) in the tropics, which is also the case in this study. Generally, increment of rainfall in this study is comparatively higher in the dry season 20.68% in the 2020s, 33.65% in 2050s, and 53.74% in 2080s for RCP8.5 scenario which might have positive impact on pastoral region of the study area and it might affect the highland areas negatively since this season is expressly main crop harvesting period.

Mann–Kendall Trend Test of Future Temperatures and Precipitation

Based on the standardized test statistic, it is possible to infer that Mann–Kendall test has revealed a statistically significant trend in the study area for both future precipitation and temperatures at the 5% significant level. The maximum and minimum temperature and precipitation for RCP2.6, 4.5 and 8.5 scenarios have revealed a significantly (at 5% significant level) increasing trend for future until the year 2100 as shown in Table 6.

Summary and Conclusion

This study tried to downscale daily temperatures and precipitation data from the CMIP5-CanESM2 output for the RCP8.5, RCP4.5, and RCP2.6 emission scenarios for future periods until year 2100 in the study area of Weyib River basin. The SDSM was used to generate future possible local Tmax, Tmin, and precipitation in the study area and it has a good ability to replicate the baseline Tmax, Tmin, and precipitation for the baseline period.

For each time slice, the change in mean annual maximum temperature has indicated a slight increment from the base period, 0.16, 0.14, and 0.15 °C for 2020s, 2050s, and 2080s, respectively, for RCP2.6 scenario, 0.12, 0.19, and

0.21 °C for 2020s, 2050s, and 2080s, respectively, for RCP4.5 scenario, and 0.12, 0.22, and 0.33 °C for 2020s, 2050s, and 2080s, respectively, for RCP8.5 scenario. For mean annual minimum temperature, the increment from the base period has been found to be 0.30, 0.43, and 0.39 °C for 2020s, 2050s, and 2080s, respectively, for RCP2.6 scenario 0.31, 0.48, and 0.57 °C for 2020s, 2050s, and 2080s, respectively, for RCP4.5 scenario and 0.34, 0.66, and 1.04 °C for 2020s, 2050s, and 2080s, respectively, for RCP8.5 scenario. The percentage change in mean annual precipitation has indicated a considerable increment from the base period 8.68, 12.93, and 11.34% for 2020s, 2050s, and 2080s, respectively, for RCP2.6 scenario, 9.54, 14.36, and 16.94% for 2020s, 2050s, and 2080s, respectively, for RCP4.5 scenario and 14.70, 19.14, and 28.69% for 2020s, 2050s, and 2080s respectively for RCP8.5 scenario.

The variability of both temperatures (maximum and minimum) and precipitation is higher for RCP8.5 than RCP4.5 and RCP2.6, and the linear trend line for all the three scenarios has indicated a significantly (at 5% significant level) increasing trend of both temperatures and precipitation for future until the year 2100. Comparatively, RCP8.5 prevails higher change in both temperatures and precipitation trend at the end of the century than the RCP4.5 and RCP2.6 scenarios. The increment of rainfall in the study area is comparatively higher in the dry season 20.68% in the 2020s, 33.65% in 2050s, and 53.74% in 2080s for RCP8.5 which might have positive impact on pastoral region of the study area and it might affect the highland areas negatively since this season is specifically main crop harvesting period.

Acknowledgements We express our heartfelt gratitude to National Meteorological Service Agency of Ethiopia (NMSAE) for providing us the meteorological data to be considered for this study.

References

- Bates B, Kundzewicz Z, Wu S (2008) Climate change and water. Technical paper of the Intergovernmental Panel on Climate Change, IPCC Secre (Geneva), 210. <http://www.citeulike.org/group/14742/article/8861411>
- Beck L, Bernauer T (2011) How will combined changes in water demand and climate affect water availability in the Zambezi river basin? *Glob Environ Change* 21(3):1061–1072
- Ethiopian National Meteorological Agency (2007) Climate Change National Adaptation Programme of Action (Napa) of Ethiopia (June). pp 1–73
- Faramarzi M, Abbaspour KC, Ashraf Vaghefi S, Farzaneh MR, Zehnder AJB, Srinivasan R, Yang H (2013) Modeling impacts of climate change on freshwater availability in Africa. *J Hydrol* 480:85–101. <http://dx.doi.org/10.1016/j.jhydrol.2012.12.016>
- Ghosh S, Mujumdar PP (2008) Statistical downscaling of GCM simulations to streamflow using relevance vector machine. *Adv Water Resour* 31(1):132–146
- Graham LP, Andersson L, Horan M, Kunz R, Lumsden T, Schulze R, Warburton M, Wilk J, Yang W (2011) Using multiple climate projections for assessing hydrological response to climate change in the Thukela River Basin, South Africa. *Phys Chem Earth* 36(14–15):727–735. <http://dx.doi.org/10.1016/j.pce.2011.07.084>

- Hamed KH (2008) Trend detection in hydrologic data: the Mann-Kendall trend test under the scaling hypothesis. *J Hydrol* 349(3):350–363
- IPCC (2013) Climate change 2013: the physical science basis. Contribution of working group I to the fifth assessment report of the Intergovernmental Panel on Climate Change. Intergovernmental Panel on Climate Change, working group I contribution to the IPCC fifth assessment report (AR5). Cambridge Univ Press, New York, p 1535
- Karpouzou D, Kavalieratou S, Babajimopoulos C (2010) Trend analysis of precipitation data in Pieria Region (Greece). *Eur Water* 30(May):31–40
- Krause P, Boyle DP (2005) Advances in geosciences comparison of different efficiency criteria for hydrological model assessment. *Adv Geosci* 5(89):89–97. <http://www.adv-geosci.net/5/89/2005/>
- Kruger AC, Shongwe S (2004) Temperature trends in South Africa: 1960–2003. *Int J Climatol* 24(15):1929–1945
- Liu L, Liu Z, Ren X, Fischer T, Xu Y (2011) Hydrological impacts of climate change in the Yellow River Basin for the 21st century using hydrological model and statistical downscaling model. *Quater Int* 244(2):211–220. <http://dx.doi.org/10.1016/j.quaint.2010.12.001>
- Nash JE, Sutcliff JV (1970) River flow forecasting through conceptual models, part I—a discussion of principles. *J Hydrol* 10:282–290
- New M, Hewitson B, Stephenson DB, Tsiga A, Kruger A, Manhique A, Gomez B, Coelho CAS, Masisi DN, Kululanga E, Mbambalala E, Adesina F, Saleh H, Kanyanga J, Adosi J, Bulane L, Fortunata L, Mdoka ML, Lajoie R (2006) Evidence of trends in daily climate extremes over southern and west Africa. *J Geophys Res Atmos* 111(14):1–11
- Shawul AA, Alamirew T, Melesse AM, Chakma S (2016) Climate change impact on the hydrology of Weyb River watershed, Bale mountainous area, Ethiopia. In: *Landscape dynamics, soils and hydrological processes in varied climates*. Springer, Berlin, pp 587–613
- Shongwe ME, Van Oldenborgh GJ, Van Den Hurk BJJM, De Boer B, Coelho CAS, Van Aalst MK (2009) Projected changes in mean and extreme precipitation in Africa under global warming. Part I: Southern Africa. *J Clim* 22(13):3819–3837
- Singh J, Knapp HV, Arnold JG, Demissie M (2004) Hydrologic modeling of the Iroquois river watershed using HSPF and SWAT. *J Am Water Resour Assoc* 41(2):343–360
- Unganai LS (1996) Historic and future climatic change in Zimbabwe. *Climate Res* 6(2):137–145
- Wilby RL, Dawson CW (2007) SDSM 4.2-A decision support tool for the assessment of regional climate change impacts, Version 4.2 user manual. Lancaster University: Lancaster/Environment Agency of England and Wales (August), pp 1–94
- Wilby RL, Dawson CW, Barrow EM (2002) SDSM—a decision support tool for the assessment of regional climate change impacts. *Environ Model Softw* 17(2):145–157. <http://linkinghub.elsevier.com/retrieve/pii/S1364815201000603>